RESEARCH ARTICLE | MARCH 25 2026

One or more holes? Comparative numerical analysis of bidirectional flow cannulas

Caterina Cara ; Francesca M. Susin ; Paolo Peruzzo

Physics of Fluids 38, 031914 (2026)
https://doi.org/10.1063/5.0314881

Physics of Fluids ARTICLE pubs.aip.org/aip/pof

One or more holes? Comparative numerical analysis of bidirectional flow cannulas

Cite as: Phys. Fluids **38**, 031914 (2026); doi: 10.1063/5.0314881
Submitted: 2 December 2025 · Accepted: 9 March 2026 ·
Published Online: 25 March 2026

Caterina Cara,[a] Francesca M. Susin, and Paolo Peruzzo

AFFILIATIONS

Cardiovascular Fluid Dynamics Laboratory, Department of Civil, Environmental and Architectural Engineering, University of Padova, Padova, Italy

[a]Author to whom correspondence should be addressed: caterina.cara@phd.unipd.it

ABSTRACT

The widespread use of veno-arterial extracorporeal membrane oxygenation (VA-ECMO) in the last decade has encouraged the concept of various return cannulas aimed at ensuring bidirectional perfusion and avoiding limb ischemia. Yet, the local hemodynamics modification owing to bidirectional flow cannulas is poorly understood. Computational fluid dynamics simulations of two different bidirectional flow cannulas inserted within an idealized artery were performed. The cannula designs differ in elbow configuration. One design has a single hole (single-hole, SH cannula), while the other has four holes (multi-hole, MH cannula) at the elbow region. Simulations were run at two different perfusion flow rates, namely, 1.4 and 3.5 L/min, and compared with the hemodynamics of a standard one-directional cannula. Both cannulas achieved improved distal perfusion compared to the standard configuration, delivering between 14% and 23%, and 22.5% and 37% of the total ECMO flow through the SH and MH configurations, respectively. However, secondary circulations arose from the distal opening, resulting in a large stagnation region along the MH cannula body. Such a condition, which is recognized as a risk factor for thrombus formation, was less pronounced in the SH solution. The analysis shows that distal openings provide adequate limb perfusion, potentially reducing ischemia risk. The multi-opening solution results in more effective outcomes to some degree but may present stagnation if not properly sized, thus potentially compromising local hemodynamics.

I. INTRODUCTION

Veno-arterial extracorporeal membrane oxygenation (VA-ECMO) has been increasingly used in the last decade as a support for patients in cardiogenic shock (CS).[1] This pathological condition is characterized by an impaired contractility of the left ventricle (LV) that induces a hypoperfusion of organs. The use of VA-ECMO ensures cardiac and gas exchange support while waiting for the patient's recovery, the implantation of a long-term support device, or heart transplantation.[2,3]

VA-ECMO consists of the following components: a centrifugal pump to provide adequate blood flow (organ perfusion), an oxygenator to enable proper gas exchange, an external tubing circuit, a drainage cannula to collect the deoxygenated blood, and a return cannula to reintroduce the oxygenated blood into the vascular system. The type of drainage and return access depends on the clinical need. This study is focused on the peripheral VA-ECMO in its femoro-femoral configuration (drainage/return access at the level of the femoral vein/artery). This type of configuration is increasingly adopted in clinical practice,[1,4] as it can be performed at the bedside without the need for an operating room. Unfortunately, the use of VA-ECMO is still associated with a high number of drawbacks[4] and a large mortality rate (ranging from 30% to 50% depending on the etiology)[5] despite the technological improvements. In particular, a high incidence of vascular complications is currently observed,[6] and these issues include increased risk of thrombus formation associated with the presence of exogenous bodies[7] and the development of abnormal flow dynamics, which can also induce a degenerative response of the vessel wall.[8–10]

The choice of the return cannula size appears to be critical in the VA-ECMO application since it is strictly dependent on the blood flow rate required for the patient's perfusion. In many cases, cannulas with a diameter comparable to that of the patient's femoral artery, i.e., the vessel where the cannula is placed, are necessary. As a result, we often witness significant occlusion and related hypoperfusion of the lower limbs, which favor the development of an ischemic condition at the level of the return access in 10%–30% of cases.[11]

To mitigate these risks, clinicians commonly use a distal perfusion catheter (DPC). This approach involves inserting a small-diameter cannula [6–8 Fr (Ref. 12)] into the return cannula at the level

of the superficial femoral artery (SFA). The added perfusion line restores blood flow to the distal limb, thereby reducing the likelihood of ischemic complications.

However, a recent study by Buda *et al.*[6] showed that the upfront use of the DPC is associated with higher mortality, suggesting its selective use. In any case, DPC requires an additional intervention and increases the risk of bleeding and infection.[13] For this reason, in recent years, return cannulas have been proposed with a new design to overcome these usage limitations.[14,15] The common feature of these cannulas is the presence of one or more secondary openings, aimed at granting distal limb perfusion. Although the multi-opening solution seems plausible and feasible, the effects of bidirectional cannulas on local hemodynamics are still poorly explored in the literature. "Are there any contraindications to using a bidirectional flow?," "Can one or more holes substantially alter hemodynamic conditions to the point of being contraindicated?" are some research questions still unanswered.

This study aims to answer the above questions through computational fluid dynamics (CFD) simulations employed to investigate the efficacy and the potential improvements associated with these types of design. Previous numerical studies on VA-ECMO have primarily focused on identifying the local implications of the watershed region position[16,17] and assessing the performance of the drainage cannula.[2,18] To our knowledge, only the work by Xi *et al.*[19] examined the hemodynamic behavior of new designs of return cannula for a representative support flow rate of 3.5 L/min. In the present work, we extend this analysis by comparing two distinct patented return cannulas under two different operating conditions: one simulating the weaning phase (laminar flow) and the other representing the target support (turbulent flow).

II. MATERIALS AND METHODS

The effectiveness of the two-flow approach in preventing limb ischemia was evaluated through a comparative analysis of two cannula designs, both derived from a one-directional configuration, hereafter referred to as the standard cannula and used as the baseline.

The cannulas have the same size with external (d_e) and internal (d) diameter equal to 21 Fr (7 mm) and 18 Fr (6 mm), respectively, and the same shape based on the arterial cannula of Edwards OptiSite (Edwards Lifesciences, Irvine, CA, USA) [Figs. 1(a) and 1(b)]. The first new cannula, labeled as SH (Single-Hole), shows a 7 Fr circular opening in the distal portion [Fig. 1(c)]. The second cannula, labeled as MH (multi-hole), features a more complex configuration in the distal portion, with four 7 Fr openings arranged around its circumference [Fig. 1(d)]. Both configurations aim to ensure secondary perfusion of the lower limb, as described in published patents.[14,15]

An idealized cannula-femoral artery district was considered to test the three cannulas' hemodynamics. Particularly, the cannula is inserted within a rigid and straight arterial segment of length, L, and diameter, D, equal to 370 and 10 mm (≈30 Fr), respectively. The cannula body is positioned in the middle of the vessel at an insertion angle equal to 35° [see Fig. 1(a)] as suggested in clinical practice.

Both cannula and vessel walls are modeled as no-slip rigid boundaries. The modeled fluid was blood with density $\rho = 1050\ \mathrm{kg/m^3}$. It is considered characterized by a Newtonian rheological law. This assumption is widely accepted in the 3D modeling of large arteries[20] and is considered appropriate here, given the focus on the femoral artery and the presence of regions, such as the vessel-cannula gap, characterized by a width greater than 0.3 mm,[21] which represents the lower limit above which the apparent viscosity may be assumed constant (i.e., consistent with a Newtonian rheological model for blood). The fluid viscosity value accounts for the hemodilution that characterizes the blood of patients undergoing VA-ECMO support, and it was set equal to $\mu = 2.8 \times 10^{-3}$ Pa·s, which corresponds to blood with 30% hematocrit and a crystalloid solution, according to the relation proposed by Eckmann *et al.*[22]

To support the circulation of patients with different degrees of cardiovascular insufficiency, the VA-ECMO device operates in a broad range of flow rates (Q = 1–7 L/min).[23] As a result, the Reynolds number in the cannula, $Re = \rho \cdot U \cdot d/\mu$, where U is the cross-sectional velocity, spans from 1000 to 9000, encompassing both laminar (Re < 2500) and turbulent (Re > 4000) regimes. To analyse the peculiarities of each hemodynamic condition, two series of simulations were carried out, each one characterized by a distinct set of boundary conditions [Fig. 1(e)]. The first series of simulations examined laminar conditions with a cannula inlet flow of Q = 1.4 L/min (Re = 1800), representing the VA-ECMO weaning phase, and a pressure gradient of 4 mm Hg was applied between the proximal and distal arterial outlets. The second series investigated the turbulent regime with an inlet flow of Q =3.5 L/min (Re = 4600), a typical setting for a 75 kg patient, and a pressure drop applied to the arterial vessel extremities equal to 10 mm Hg.

The introduced pressure drops are important to ensure a reasonable flow direction in both regimes; the higher value in the turbulent case is consistent with the increased dissipation inherent to the regime.

The flow field is fully described by the Navier–Stokes and the mass conservation equations, which, respectively, read

$$\nabla p = -\rho d \frac{\vec{\mathbf{u}}}{dt} + \mu \nabla^2 \vec{\boldsymbol{u}}, \tag{1}$$

$$\nabla \cdot \vec{\boldsymbol{u}} = 0. \tag{2}$$

Here, p is the pressure, and $\vec{\mathbf{u}}$ is the blood flow velocity.

Fluid dynamics is simulated using COMSOL Multiphysics®. The laminar regime is solved through direct numerical simulation (DNS), while the turbulent regime is reproduced using large eddy simulation (LES). The residual-based variational multiscale (RBVM) method[24] is adopted to have a more detailed description of the unresolved eddy scales (see Subsection 1 of Appendix A).

The suitability of the fluid domain discretization was assessed through a mesh sensitivity analysis, with the aim of obtaining a good trade-off between computational cost and accuracy (see Subsection 2 of Appendix B). The flow domain is discretized with a similar number of elements for all the cases, resulting in a mesh of nearly 3 130 000 and 4 000 000 linear tetrahedra for the laminar and turbulent scenarios, respectively. The higher number of elements in the turbulent simulations is due to the introduction of the boundary layer along the cannula surface and in the vessel's regions near the cannula outlet and elbow (Fig. 2). The mesh size ranges from 0.35 to 1.00 mm in the bulk regions, while the boundary layer is composed of six layers, with the smallest size equal to 0.04 mm. The evaluation of the element quality, based on the skewness parameter, yielded an average and minimum value of 0.66 and 0.19, respectively.

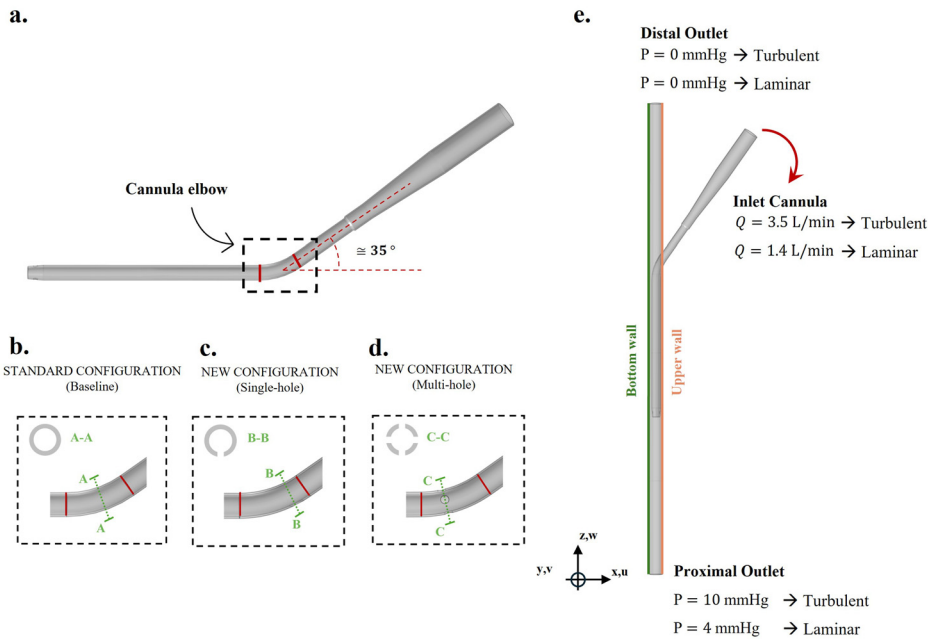

FIG. 1. Fluid domain geometry. Schematic description of the three flow cannula solutions, with the assigned coordinate system (*x, y, z*) and velocity components (*u, v, w*), respectively. (a) Representation of the cannula schematization, evidencing the elbow region. (b)–(d). Details of the elbow region for the baseline, SH, and MH configurations. (e) Sketch of the femoral artery-cannula district with details of the BCs used in the simulations.

Globally, the simulated period of each simulation is 3 s. In all runs, the system starts from Q = 0 L/min, and the target flow is reached within 0.5 s through a ramp. The target flow (1.4 or 3.5 L/min, depending on the regime) is then maintained for an additional 2.5 s, in order to minimize the impact of transient flow effects on the distal results (see Subsection 3 of Appendix C).

III. RESULTS

A. Velocity field

The analysis of the velocity field highlights the significant impact of cannula introduction on hemodynamics and its potential role in the development of nonphysiological conditions due to disturbed flow.[25]

1. Laminar condition

Figure 3 illustrates the velocity magnitude, *U*, in the *zx*-plane for the three cannulas, highlighting distinct flow patterns in the proximal and distal regions of the arterial vessel.

The baseline configuration exhibits a high-velocity jet at the cannula outlet within the central region of the vessel's proximal segment, with an irregular flow distribution. In contrast, the distal part of the vessel, which is the critical region of the domain for evaluating the design's effectiveness in preventing ischemic conditions, shows a more uniform distribution of the flow in the *zx*-plane view [Fig. 3(a)]. The presence of this slight distal perfusion is solely due to the small gaps maintained between the cannula and the vessel wall in the simulations.

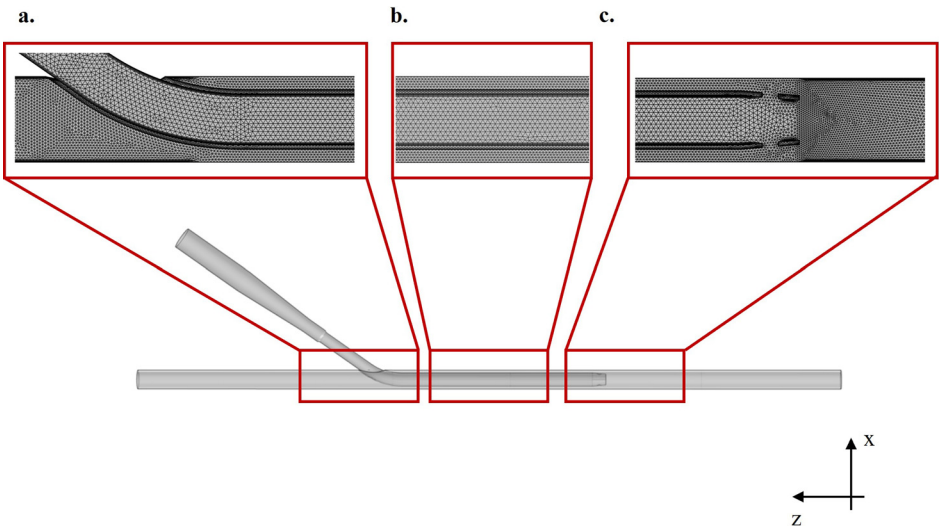

FIG. 2. Mesh distribution in different areas of the fluid domain. Highlighting the areas with boundary layer in panels (a) and (c), while panel (b) shows the mesh distribution in the vessel-cannula gap.

The flow distribution is quite different adopting the new cannula designs, with only some qualitative similarities as can be easily seen comparing the velocity patterns in the three insets of Fig. 3. In the proximal region, the SH cannula shows a disturbed flow pattern similar to that of the baseline, whereas a more uniform jet is found in the MH cannula. Conversely, in the distal region, the SH cannula shows a complex flow structure as a result of the high velocity jet through the secondary opening, while in the MH cannula, the velocity appears more uniformly distributed as observed in the baseline. The differences encountered in the two new designs can be attributed to the number and distribution of the holes. In the SH cannula, the presence of a single hole leads to a high-intensity jet in the distal part, but this does not significantly attenuate the flow rate along the proximal portion of the cannula, thus leading to disturbed distributions of the blood velocity in both regions of the artery. In contrast, in the MH cannula, the blood flow through each hole is smaller than in the SH case; however, overall, we observe a strong reduction of the flow through the

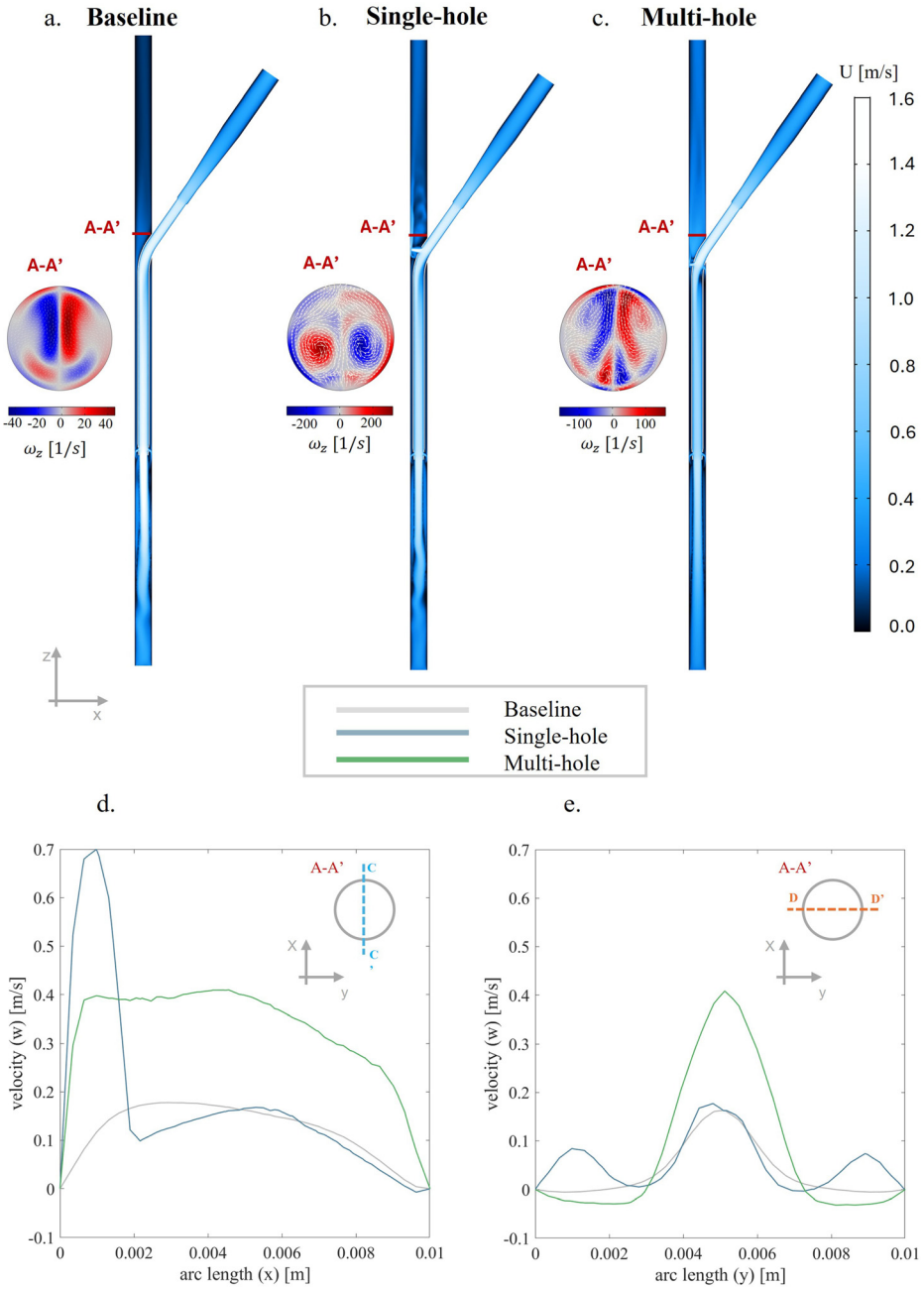

FIG. 3. Assessment of the velocity field under laminar flow conditions. (a)–(c) Velocity distribution in the zx-plane in the three cannulas, while the out-of-plane vorticity is reported in the A-A' cross section. (d) and (e) Velocity profiles computed in Section A-A' along segments C-C' and D-D' (see insets) for the three cases.

main body of the cannula downstream of the elbow, thus resulting in a more uniform velocity distribution across both vessel segments.

Nevertheless, in all configurations, disregarding the presence of secondary holes, the most extended high-velocity region is observed in the proximal portion of the artery, near the main outflow. Here, the velocity peaks are equal to 1.21 and 1.0 m/s for cases SH and MH, respectively. However, these values are lower than those observed in the baseline condition 1.55 m/s, where the entire blood flow is directed through the proximal outlet.

An analysis of the out-of-plane vorticity (ω_z) in the $A - A'$ section, positioned at the level of the cannula insertion point in the vessel, shows the development of vortical structures, with enhanced values in the MH and SH cannula. Specifically, the peak of the out-of-plane vorticity increases from the range of $[-40,+40]$ s^{-1} in the baseline configuration to $[-200, +200]$ s^{-1} in the SH and $[-100, +100]$ s^{-1} in the MH cannulas. This increase in ω_z is related to the impingement of the ECMO jet in this area, attributed to the side holes positioned at the level of the elbow. The presence of these secondary flows results in a highly three-dimensional flow field, as demonstrated by the evaluation of the streamwise velocity component along two different directions of the $A - A'$ section. In the $C - C'$ segment [Fig. 3(d)] a nearly uniform streamwise velocity component w has been identified in most part of the cannula, as in the baseline condition, in both bidirectional cannulas, but with different velocity values (0.18 m/s in the baseline, 0.17 in the SH cannula, and 0.41 m/s in the MH cannula); the SH cannula presents an exception with a localized peak near the bottom of the vessel (≈0.7 m/s). While the evaluation of w in the $D - D'$ segment [Fig. 3(e)] highlights a heterogeneous behavior. Similar to the baseline condition, the cannula MH exhibits a preferential flow region in the central portion of the vessel (≈0.4 m/s, while in the baseline, it is equal to 0.16 m/s), along with slight negative velocities near the wall (≈−0.03 m/s). In contrast, the SH cannula pattern exhibits three distinct velocity peaks—near the wall and in the central portion—ranging between 0.08 and 0.17 m/s. Despite the improvements obtained in the distal part, all measured values remain lower than 1.15 m/s that corresponds to the physiological references for the systolic peak of velocity at the level of the common femoral artery in healthy conditions.[26] In addition, these values are lower than the mean forward velocity component (Common Femoral artery 69.73 ± 3.96 cm/s, Superficial Femoral Artery 70.26 ± 3.38 cm/s, and Profunda Femoris Artery 51.74 ± 2.95 cm/s).[27]

2. Turbulent condition

The increase in flow inertia, i.e., the Reynolds number, is responsible for irregular velocity patterns in the proximal portion of the artery, regardless of the type of cannula. Conversely, by evaluating the distal portion of the vessel, a significant difference between the baseline condition and the new generation cannulas emerges, as reported in Fig. 4. Specifically, in the baseline case, the flow distribution in the distal segment is similar to that identified in the laminar condition, whereas both new cannulas exhibit a highly disturbed flow pattern due to the increased flow at the cannula inlet. Also, in this scenario, the most extended high velocity area is at the level of the main outflow of the cannula, with velocity peaks at t = 3 s equal to 3.46 and 3.38 m/s in the SH and MH cannula, respectively. Both values are lower than the velocity estimated in the baseline configuration, which is equal to 4.04 m/s. In the current hemodynamic regime, particular attention should be given to the flow field within the cannula. Low velocity areas are identified in the baseline and the SH configuration in the upper part of the cannula body [see Fig. 4, panels (a) and (b)], while the MH cannula shows a highly disturbed flow throughout the section [Fig. 4(c)]. The evaluation of the velocity profile (w-velocity component) in the distal part of the vessel is reported in Fig. 4 [panels (d), (e), (f), (g)] to assess how turbulent conditions affect the velocity distribution in the new-generation cannulas and how these dynamics may help to prevent the onset of ischemic conditions. This analysis is particularly relevant, considering that the behavior of the baseline configuration in the distal region appears to be independent of the flow regime; indeed, the increase in the flow at the inlet of the cannula does not produce any effect in the distal region of the vessel. The results report the mean ± standard deviation of the outputs and underscore irregular hemodynamic conditions both in space and time. Notably, the vertical velocity profile [$C - C'$, panels (d) and (e)] shows that the higher velocity region in both the SH and MH cannula is near the bottom of the vessel. Specifically, the SH cannula has two distinguished peaks with the higher near the bottom of the vessel (1.32 ± 0.54 m/s and 0.94 ± 0.47 m/s, respectively), while the MH cannula shows a single peak (0.58 ± 0.17 m/s).

The dynamics appear more complex along the transverse direction [$D - D'$, panels (f) and (g)], especially for the single-hole configuration, where alternating backflows and forward flows mark out the hemodynamics.

B. Pressure drop

The introduction of secondary perfusion openings also impacts flow resistance along the cannula, overall resulting in a pressure head reduction with respect to the baseline configuration once a fixed flow rate Q is prescribed in VA-ECMO (Fig. 5). In the laminar case, the above difference is estimated to be approximately 5.5 and 8.0 mm Hg for the Single-Hole and Multi-Hole cannula, respectively. As expected, the reduction in pressure loss downstream of the secondary holes mirrors the corresponding reduction in flow rate in the final section of the cannula. Interestingly, this corresponds to a significant reduction in the mean velocity through the elbow, while the total mechanical energy of the flow remains unchanged. As a result, pressure is recovered along the elbow, which represents the signature of localized leakage in the upstream section. Specifically, the higher the pressure recovery, the higher the flow rate through the distal outlet, thus suggesting a larger amount of blood flowing toward the limb in the multi-hole scenario compared with the single-hole case.

Finally, while we observe a more-than-linear increase in pressure with Q from the laminar to the turbulent regime no substantial change is observed in the pressure distribution along the cannulas across the two series of experiments.

C. Shear stress

The time-averaged wall shear stress, $\bar{\tau}_w$, is another key parameter for assessing local hemodynamics. Figure 6 displays the wall shear stress distribution normalized with the critical shear stress $\tau_c = 0.4$ Pa, i.e., the stress value below which the triggering of the biochemical processes associated with hyperplasia of the tunica intima, the innermost layer of the artery endothelium, is observed.[28,29]

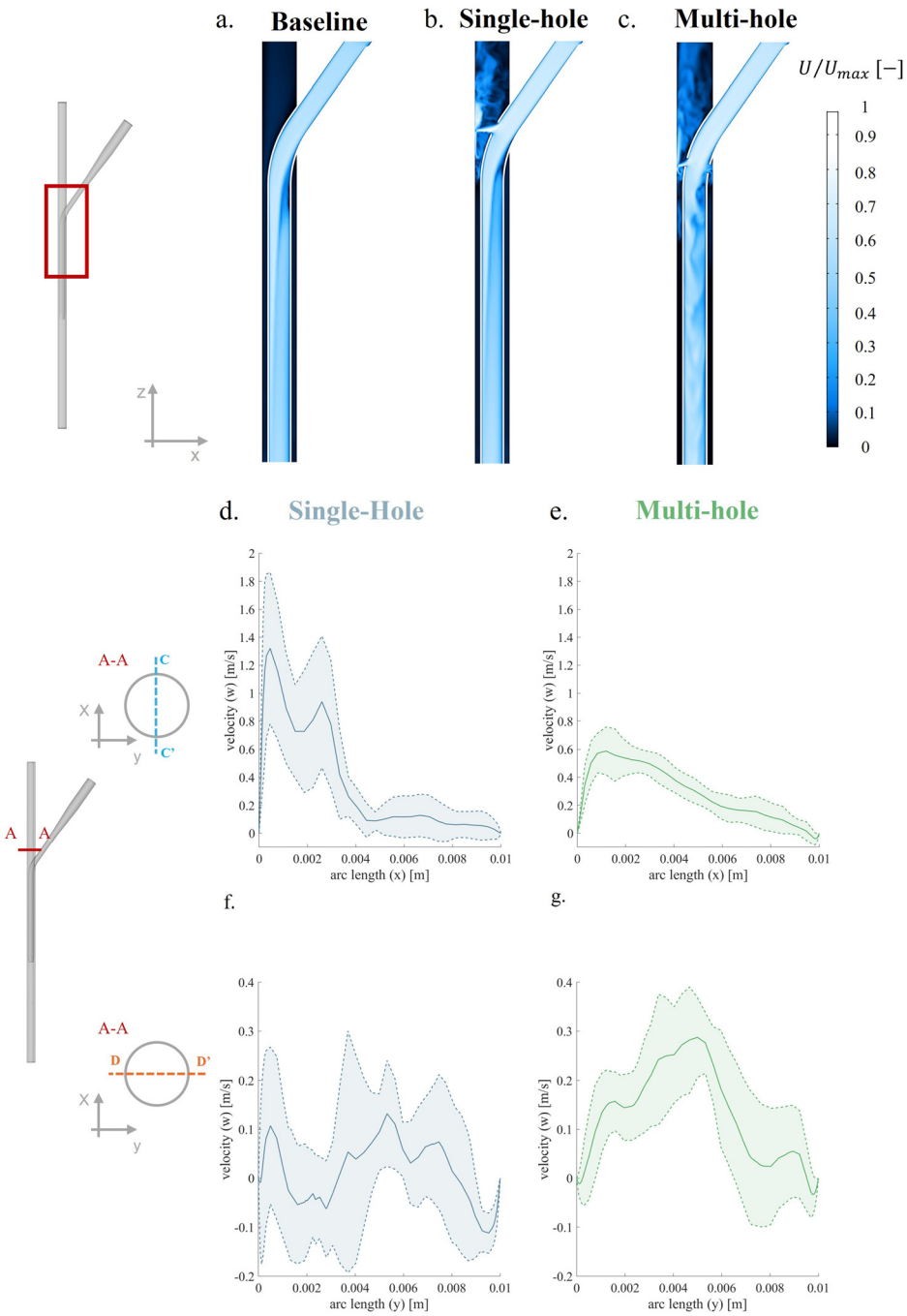

FIG. 4. Assessment of the velocity field under turbulent flow conditions. (a)–(c) Velocity distribution in the distal part of the vessel and in the main part of the cannula body. (d) and (e) Velocity profile along C-C' direction (see inset) in SH and MH cases. (f) and (g) Velocity profile along D-D' direction (see inset) in SH and MH cases. The results in panels (d)–(g) are reported as mean over 1 s ± standard deviation (sd).

Only regions with shear stress $\tau^* = \bar{\tau}_w/\tau_c < 1$ are reported in the figure for the sake of clarity. Panels (a) and (d) of Fig. 6 show the behavior of the baseline cannula under both the hemodynamic regimes, evidencing no significant differences, as shown in the case of the velocity field. The baseline configuration shows an extended low τ^* region in the distal part of the vessel, suggesting a potential risk of abnormal wall response. Marked differences from the baseline configuration are observed in the two new cannula designs with regime-dependent patterns. Under laminar flow, the entire artery is affected by potentially damaging τ^* when the multi-hole cannula is inserted [panel (b)]. The adoption of the single-hole cannula mitigates the extension of low-stress regions [panels (a) and (c)], which are substantially limited to the distal portion of the artery.

The persistence of low wall shear stress is not observed in turbulent scenarios, where higher Q increases τ^* in both the proximal and distal regions. Notably, in the MH cannula, stagnation of blood with

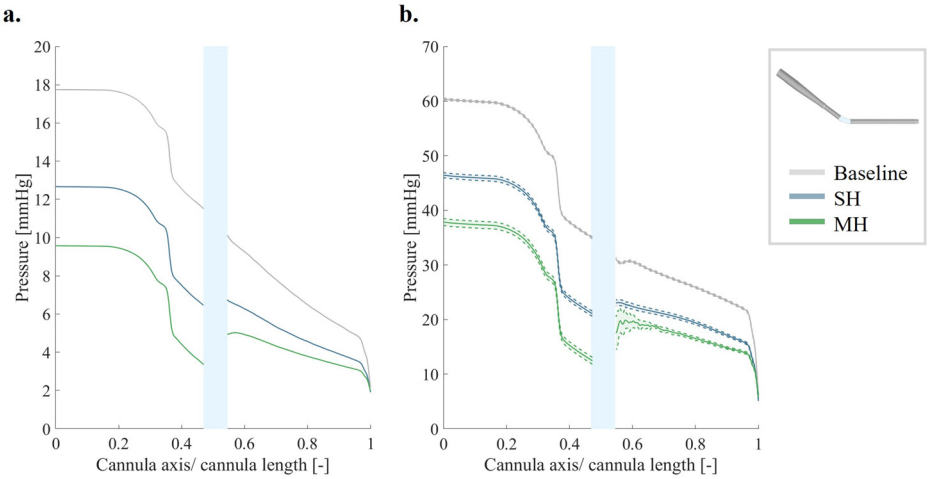

FIG. 5. Pressure drop along the axis of the cannulae for (a) laminar and (b) turbulent regimes.

$\tau^* \approx 0$ occurs along the portion of the artery occupied by the cannula (panel f). Such a condition is likely caused by flow recirculation around the cannula body, fed by the outlets positioned on the elbow. This is particularly effective in hindering the mass exchange between the proximal and distal portions of the artery, as highlighted in Fig. 7, which displays the shear rate $\dot{\gamma}$ and the in-plane velocity vectors in the four scenarios analyzed.

D. Performance of the different cannulas

In the present analysis, the cannula partially occluded the hosting artery, maintaining a small gap between its body and the vessel wall. Accordingly, a non-null flow rate toward the lower limb can also be established in the absence of secondary outlets (baseline scenario). Here, to estimate the distal flow rate, Q_{elbow}, we first assess the blood flow through the openings on the cannula elbow. In the laminar simulations, Q_{elbow} equals 0.32 L/min for the single-hole configuration and 0.52 L/min for the multi-hole cannula. This means that the fraction of the VA-ECMO flow rate feeding the limb is nearly 23% and 37% in the two cases, respectively. In the turbulent cases, the increment of Q determines the increment of Q_{elbow} in both the cannula SH and MH, resulting $Q_{elbow} = 0.50$ and 0.79 L/min, respectively. However, the above absolute increment corresponds to a reduction of the fraction of Q toward the limb (14.2% and 22.5% for Cannula SH and MH, respectively), as shown in Fig. 8.

The assessment of the flow in the distal portion (Q_d) of the vessel shows, in the baseline configuration, a $Q_d = 0.24$ L/min in both the hemodynamic regimes. In this case, the perfusion is entirely provided by the blood flowing through the gap between the cannula and the arterial wall. In cannula SH, Q_d is equal to 0.51 L/min with the cannula-artery gap contributing approximately 36% of the total distal perfusion. In the MH-cannula, the distal flow is equal to 0.59 L/min, with the gap accounting for only 12% of the total. In both configurations, a reduction of approximately 10% of the cannula-gap contribution to the distal flow is identified in the turbulent case. The low vessel-cannula gap contribution that characterizes the MH-cannula can be attributed to the vortices created by the presence of the four holes, as shown in Fig. 7. The results for the SH and MH designs indicate that the distal perfusion delivered by bidirectional cannulas cannot be predetermined, and this is in agreement with the findings of Simons *et al.*[11]

IV. DISCUSSION

In patients undergoing VA-ECMO, inserting a return cannula into the femoral artery significantly alters physiological blood circulation due to the external pump supporting cardiac function. Additionally, the cannula itself obstructs the artery, severely limiting limb perfusion [Fig. 3(a)]. For this reason, a comparative analysis between the standard cannula and innovative cannula configurations is conducted. The new generation designs are characterized by the presence of secondary openings that promote distal perfusion in both the laminar and turbulent flow regimes [Figs. 3(b) and 3(c) and Fig. 4]. While such an outcome is expected, our numerical simulations reveal unexpected and sometimes counterintuitive results.

In both simulated scenarios, the single-hole configuration intensifies the three-dimensional nature of the flow, showing a behavior significantly different from that observed in the baseline configuration. The presence of a highly three-dimensional flow enhances the cannula backside flushing even at a low flow rate Q, showing limited areas with low τ^* [see Fig. 6(b)]. In contrast, in the laminar regime, the multiple-opening configuration, facilitated by diffusive leakage around the elbow, shows a flow velocity condition, which resembles those observed in the baseline configuration. However, in the turbulent scenario, the increase in flow velocity through the secondary holes virtually excludes the distal from the proximal region of the artery (Fig. 7), leading to results that differ from the baseline case. It remains unclear whether this could lead to some benefits in the efficacy of the treatment, as the limb perfusion turns out to be weakly dependent on the vessel size. Nonetheless, the shear stress distribution reported in Fig. 6 [panel (f)] indicates higher risks of thrombogenicity near the insertion site.

The evaluation of the shear stress, τ, in the cardiovascular system is particularly important, as it is the main variable that mediates the physiological signaling in wall cells.[10] In fact, abnormal distributions or values of τ are usually associated with a non-physiological response of the vessel wall. The shear-dependent phenomena have a higher impact on the arterial system[30,31] than on the venous one; therefore, the assessment of this hemodynamic parameter seems important in the present study, where abnormal flow patterns emerge within the arterial-cannula district. In the standard cannula configuration, areas with low values of τ^* are identified in the distal part of the vessel [Fig. 6, panels (a) and (d)], suggesting a potential worsening in the ischemic condition.

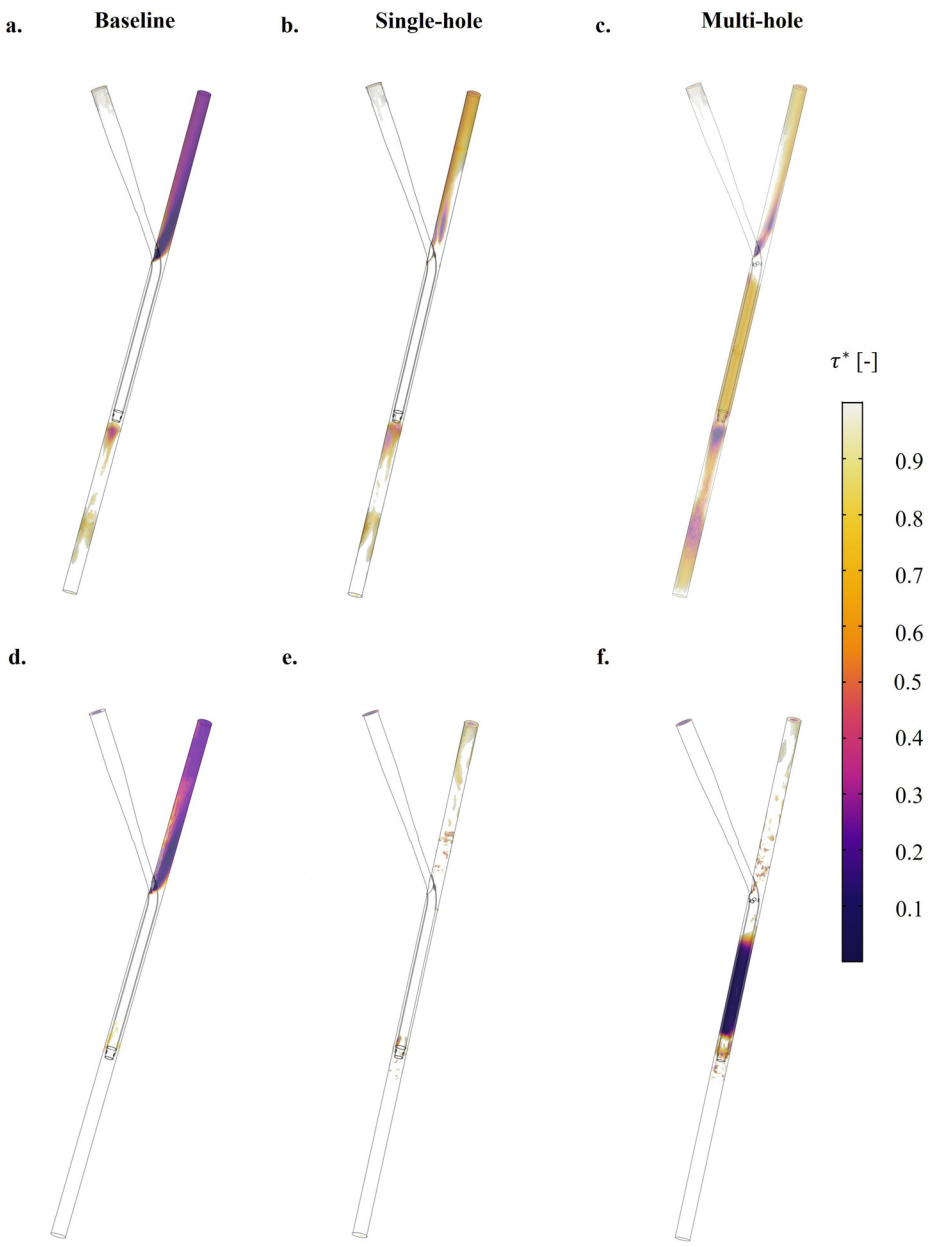

FIG. 6. Shear stress in the two analyzed hemodynamic regimes. Normalized shear stress τ^* along the artery under laminar conditions: (a)–(c); and under turbulent conditions (d)–(f). In turbulent flow, values of τ^* are averaged over the last 1 s of simulation.

A similar behavior is evident in the MH cannula, under the laminar regime, where the diffusive leakage created by the four holes leads to an abnormal response of the wall not only at the distal but also at the level of the proximal part of the vessel. Conversely, the SH cannula, thanks to a concentrated Q_{elbow} in a single hole, seems to promote more favorable conditions along the artery. At low Q, it generates sufficient backward recirculation and consistently maintains perfusion through the proximal outlet. At high Q, it allows for potential blood flow through the gaps between the cannula and the artery.

Proper sizing of the secondary holes in MH-configuration can help achieve results comparable to those of SH cannula, leading to improved distal perfusion. Nonetheless, substantial distal diversion of flow can be advantageous, as it may reduce the hydraulic resistance within the cannula and lessen the mechanical stress exerted on blood cells during their passage through both the device body and the openings.[32] In all configurations, platelet activation and endothelial damage may occur due to the formation of high shear rate regions near the secondary outlets ($\dot{\gamma} > 5000\ s^{-1}$),[10,33] particularly under turbulent flow conditions. As illustrated in Fig. 7, a reduction of the area extension is evidenced with increasing number of holes at the level of the elbow. Moreover, the analysis reveals localized zones where $\dot{\gamma}$ reaches values as high as 50 000 s^{-1}. Whether such extreme shear rates could lead to hemolysis remains uncertain, as this also depends on the duration of red blood cell exposure to altered conditions. Given the complexity of the phenomenon,

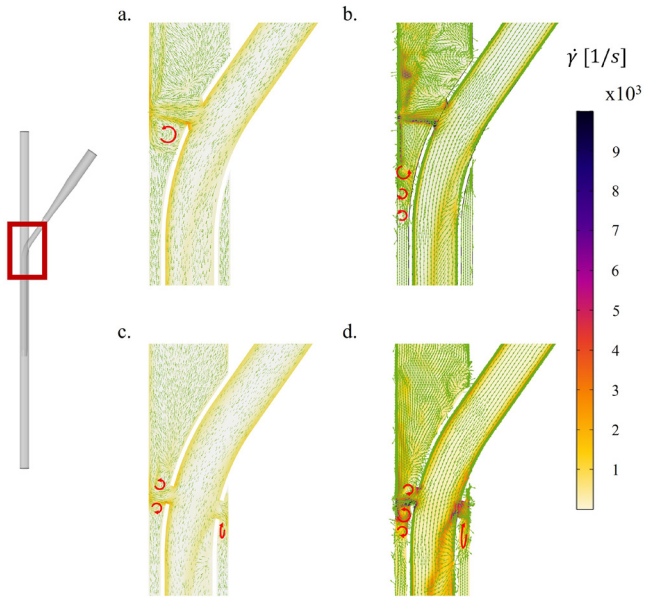

FIG. 7. Assessment of the shear rate and the velocity field (green arrow vectors) in the two configurations of bi-flow cannula. Shown are the SH (a) and (b) and MH (c) and (d) configurations under laminar (a) and (c) and turbulent (b) and (d) conditions. For turbulent cases, the results are time-averaged over the last second of simulation.

further specific studies are required to assess the hemolytic potential of present cannula configurations (see, e.g., Marom and Bluestein[32]). In any case, the proper sizing of the secondary openings must also account for this aspect, balancing all the factors mentioned above.

At this stage, a comprehensive experimental or clinical validation is not feasible. Nevertheless, the numerical findings show qualitative agreement with previous studies on alternative cannula designs, such as those reported by Xi *et al.*[19] (e.g., low velocity and shear stress areas), as well as with preliminary observations from the clinical use of similar devices.[34] The regions with low velocity and low shear stress recognized in the present analysis agree with those reported in Xi *et al.*[19] In that work, the

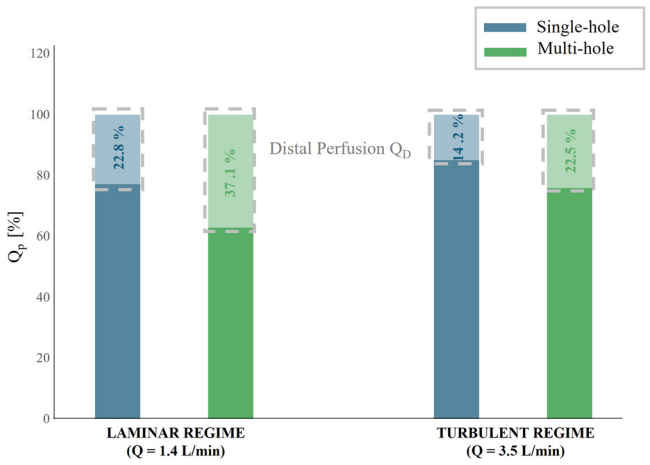

FIG. 8. Flow distribution in distal (Q_d) and proximal (Q_p) part of the vessel for the two bi-directional cannulas under laminar and turbulent conditions.

authors demonstrated that cannula designs promoting distal perfusion can reduce the risk of blood stagnation (i.e., residence time) under VA-ECMO conditions ($Q = 3.5$ L/min), thereby decreasing the hemolysis index. However, the pressure drop predicted in Xi *et al.*[19] is quite higher than that obtained in the present study. This is likely due to their adoption of the $k - \omega$ Reynolds-Averaged Navier-Stokes (RANS) formulations, which implicitly assumes a fully developed turbulent regime throughout the domain and may thus lead to overestimating the viscous dissipations along both the cannula and the vessel. In contrast, the adoption of the RBVM-based LES employed here provides a more faithful representation of the local hemodynamics, and consequently of the losses and the pressure drop associated with the cannula.

A preliminary comparison of the distal perfusion improvement can be made between the present results and clinical outcomes on the BiFlow cannula (LiVanova, Italy), which utilizes the same bidirectional flow concept as the single-hole solution proposed here. Gunaydin *et al.*[34] reported blood flow rates measured in 15 patients undergoing VA-ECMO with a 19 Fr BiFlow cannula. In this cohort, Doppler ultrasonography revealed that 33.1% of the total flow rate was directed along the limb with an external blood perfusion of 2.2–2.5 L/min per m^2. This operating condition is not significantly different from the turbulent scenario simulated in our study. The percentage of flow along the distal portion of the artery exceeds the 14.2% computed for the secondary hole alone, aligning more closely with the total flow distribution in our simulation, which accounts for contributions from the secondary outlet and the cannula-artery gaps, estimated at 27.2%.

Although the satisfactory comparison, applying our estimation to a real-world scenario requires caution for several reasons. First, the boundary conditions used in our simulations do not accurately replicate the actual pressure in a patient under VA-ECMO, which could result in a different distribution of flow rates along the proximal and distal directions. In addition, they are maintained constant along all the simulated time, so no differences in the flow distribution can be identified based on the specific phase of the cardiac cycle. Second, real arteries exhibit mechanical properties that may lead to local lumen compression owing to the cannula insertion.[35] and compliance-related effects on pressure and flow propagation—factors that can result in additional local hemodynamic alterations not captured in our model.[36,37] Third, the anatomical geometry of real arteries is likely to influence cannula positioning, particularly regarding gap distribution and the positioning of the distal opening. The extent to which these factors may affect flow partitioning remains unquantified and warrants further investigation. Finally, while the assumption of Newtonian rheology is justified by the shear rate values observed in this study, the adoption of non-Newtonian models should be considered if the gap between the cannula and the vessel is significantly reduced. Despite this, the persistence of small pressure differences at the artery extremities during diastole is expected; accordingly, our results should be regarded as representative of the hemodynamics in this specific phase of the cardiac cycle. However, to address the aforementioned limitations, coupling the present 3D CFD model of the return cannula–femoral artery district with a lumped-parameter (0D) model of the global cardiovascular system appears to be a promising strategy for imposing physiologically realistic boundary conditions and for assessing the efficacy of the bidirectional flow solution.[38] Such a coupled approach would also enable the investigation of the broader hemodynamic impact of VA-ECMO—both local and

systemic—particularly in scenarios involving impaired ventricular function.[39] We believe that the development of such an advanced numerical tool would offer significant benefits to clinicians, aiding both in patient monitoring and therapeutic planning during VA-ECMO support. The present work represents an initial step toward achieving this ambitious purpose.

V. CONCLUSIONS

In this study, we characterized the hemodynamics near the return access of two types of bidirectional cannulas properly designed for VA-ECMO treatment, in comparison with a standard cannula design.

Specifically, the first cannula shows a single distal opening, while the second solution includes more distal holes. We assessed the cannula performance through a series of 3D numerical simulations exploring two distinct flow regimes, namely, laminar ($Q = 1.4$ L/min) and turbulent ($Q = 3.5$ L/min).

The numerical analysis underscores that secondary distal openings ensure adequate blood perfusion along the limb, thereby reducing the risk of ischemia often associated with using VA-ECMO. The perfusion we estimated with a single-hole configuration is consistent with the clinical measurements observed in patients using a commercial cannula with a similar bidirectional flow solution. However, the effectiveness of the flow rate repartition seems influenced by many factors; among the others, the amount of blood flow pumped by the VA-ECMO, whose increment determines a reduction in the proportion of blood directed toward the limb.

Although the cannula design with multiple openings promotes more homogeneous flow conditions in the distal portion of the artery, our preliminary simulations do not reveal any substantial benefits from its use. On the contrary, the results suggest that such designs require careful sizing of the secondary openings to avoid the formation of a large stagnation region, which may adversely affect local hemodynamics and result in performance comparable to the baseline design, thereby limiting its potential advantage.

ACKNOWLEDGMENTS

This work was developed under the framework of the Infrastructure of Research of the University of Padova, INCAS. The author would like to thank Gianmarco Boscolo for the helpful and stimulating discussion on this topic.

AUTHOR DECLARATIONS

Conflict of Interest

The authors have no conflicts to disclose.

Author Contributions

Caterina Cara: Data curation (equal); Formal analysis (equal); Investigation (equal); Methodology (equal); Visualization (equal); Writing – original draft (equal). **Francesca M. Susin:** Conceptualization (equal); Supervision (equal); Writing – review & editing (equal). **Paolo Peruzzo:** Conceptualization (equal); Formal analysis (equal); Methodology (equal); Supervision (equal); Writing – original draft (equal).

DATA AVAILABILITY

The data that support the findings of this study are available from the corresponding author upon reasonable request.

APPENDIX A: TURBULENCE MODELING STRATEGY

1. Turbulence modeling strategy

The flow field in the cannula vessel return district is fully described by the Navier–Stokes equations and the mass conservation, which, respectively, read

$$\nabla p = -\rho d\frac{\vec{\mathbf{u}}}{dt} + \mu\nabla^2\vec{\boldsymbol{u}}, \tag{A1}$$

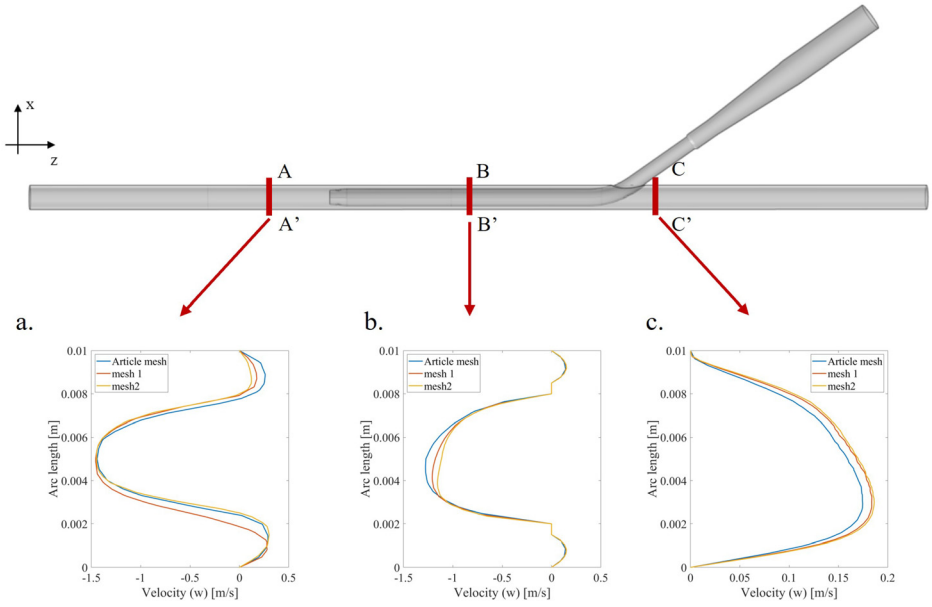

FIG. 9. Assessment of the velocity profile along the vessel in three significant cross sections of the fluid domain. Article mesh: mesh used in the article, mesh 1: first refinement, mesh 2: second refinement.

$$\nabla \cdot \vec{\mathbf{u}} = 0. \quad \text{(A2)}$$

Here, p is the pressure, $\vec{\mathbf{u}}$ is the blood flow velocity, ρ is the fluid density ($\rho = 1050\,\text{kg/m}^3$), and μ is the dynamic viscosity ($\mu = 2.8 \times 10^{-3}$ Pa s). Fluid dynamics in the cannulas is simulated using COMSOL Multiphysics®. The laminar regime is solved through direct numerical simulation (DNS), while the turbulent regime is reproduced using large eddy simulation (LES). The residual-based variational multiscale (RBVM) method[24] is adopted to have a more detailed description of the unresolved eddy scales, i.e., the residuals of the resolved scales are used to obtain velocity (u') and pressure (p') fluctuations as

$$\boldsymbol{u}' = -\tau_m \cdot \boldsymbol{res_m}, \quad \text{(A3)}$$

$$p' = -\tau_c \cdot res_c, \quad \text{(A4)}$$

where

- res_m is the momentum equation residual, expressed as

$$\boldsymbol{res_m} = \rho\left(\frac{\partial \boldsymbol{u}}{\partial t} + \boldsymbol{u} \cdot \nabla \boldsymbol{u}\right) + \nabla p - \nabla \cdot \left[\mu\left(\nabla \boldsymbol{u} + (\nabla \boldsymbol{u})^T\right)\right], \quad \text{(A5)}$$

- res_c is the continuity equation residuals, expressed as

$$res_c = \rho \nabla \cdot \boldsymbol{u}. \quad \text{(A6)}$$

- τ_m is the intrinsic time-scales of the momentum equation and is expressed as

$$\tau_m = \frac{1}{\sqrt{\left(\frac{C_1 \rho}{\Delta t}\right)^2 + 4\rho^2 \boldsymbol{u} \cdot \boldsymbol{G}\boldsymbol{u} + C_2 \mu^2 \mathbf{G} : \mathbf{G}}}, \quad \text{(A7)}$$

with C_1 being a constant depending on the temporal scheme, C_2 is a constant depending on the shape of the element, and **G** is the covariant matrix tensor;

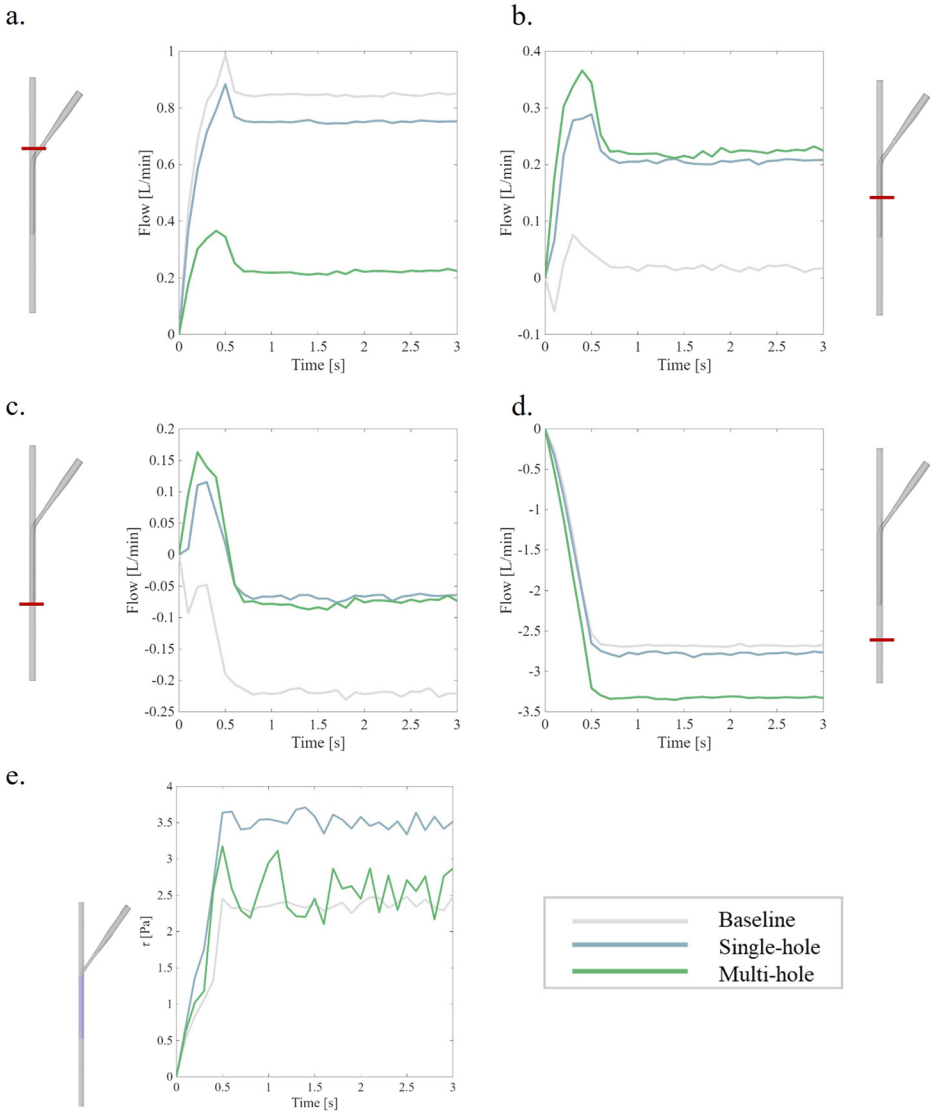

FIG. 10. Assessment of result stationarity. Panels (a)–(d) display the flow rate stability across four different sections in the three cannula configurations, while panel (e) illustrates the steadiness of the wall shear stress (τ) within a specific region of interest.

- τ_c is the intrinsic time-scales of the continuity equation and is expressed as

$$\tau_c = C_3(\rho\tau_m trace(\boldsymbol{G}))^{-1}, \tag{A8}$$

with C_3 being a constant depending on both the order of the shape function and the shape of the element.

The parameters C_1, C_2, and C_3 are algorithmic constants,[40] automatically set by COMSOL Multiphysics® based on the numerical formulation of the problem.

APPENDIX B: MESH SENSITIVITY

In the present study, the mesh sensitivity was explored considering the baseline configuration under laminar flow regime. The results in the three evaluated meshes (article mesh: 3 131 632 elements, 1st mesh refinement: 6 012 899 elements, 2nd mesh refinement: 8 664 874 elements) exhibited consistent flow patterns, demonstrating that all configurations effectively capture the main hemodynamic features (Fig. 9). Despite the substantial increase in the number of elements, only minor quantitative differences were observed. In particular, the variation between the mesh adopted in the study (the coarsest one) and the finest mesh was below 8% for both distal flow rate and mean wall shear stress, which are the main variables of interest in the present study. This discrepancy is considered acceptable given the inherent modeling assumptions and ensures an optimal balance between numerical accuracy and computational efficiency.

APPENDIX C: STATIONARY CONDITION

The achievement of a statistically steady condition and boundary layer stability in the turbulent regime is confirmed by evaluating the time evolution of the flow in different sections of the vessel [Figs. 10(a)–10(d)], as well as monitoring the surface averaged wall shear stress along the vessel surface [Fig. 10(e)]. Both metrics oscillate around a constant mean value without significant drift, confirming that the transient phase is exhausted.

REFERENCES

[1]Extracorporeal Life Support Organization, see https://www.elso.org/registry/internationalsummaryandreports/internationalsummary.aspx for "ELSO international summary of statistics" (accessed July 16, 2025).

[2]A. Wickramarachchi, S. D. Gregory, A. J. Burrell, and M. Khamooshi, "Flow characterization of maquet and bio-medicus multi-stage drainage cannulae during venoarterial extracorporeal membrane oxygenation," Comput. Biol. Med. **171**, 108135 (2024).

[3]G. Singh, D. Hudson, and A. Shaw, "Medical optimization and liberation of adult patients from va-ecmo," Can. J. Cardiol. **36**, 280–290 (2020).

[4]A. Tsangaris, T. Alexy, R. Kalra, M. Kosmopoulos, A. Elliott, J. A. Bartos, and D. Yannopoulos, "Overview of veno-arterial extracorporeal membrane oxygenation (VA-ECMO) support for the management of cardiogenic shock," Front. Cardiovasc. Med. **8**, 686558 (2021).

[5]A. C. Alba, F. Foroutan, T. A. Buchan, J. Alvarez, A. Kinsella, K. Clark, A. Zhu, K. Lau, C. McGuinty, N. Aleksova *et al.*, "Mortality in patients with cardiogenic shock supported with VA ECMO: A systematic review and meta-analysis evaluating the impact of etiology on 29,289 patients," J. Heart Lung Transplant. **40**, 260–268 (2021).

[6]K. G. Buda, E. C. Robinson, J. Titus, P. M. Eckman, I. Chavez, E. Cravero, L. Stanberry, and K. Hryniewicz, "Routine versus selective distal perfusion catheter use in venoarterial extracorporeal membrane oxygenation," ASAIO J. **71**, 36–1097 (2025).

[7]J. Fraser, K. Shekar, S. Diab, K. Dunster, S. Foley, C. McDonald, M. Passmore, G. Simonova, J. Roberts, D. Platts *et al.*, "ECMO–the clinician's view," ISBT Sci. Ser. **7**, 82–88 (2012).

[8]J. Thomas, V. Kostousov, and J. Teruya, "Bleeding and thrombotic complications in the use of extracorporeal membrane oxygenation," in *Seminars in Thrombosis and Hemostasis* (Thieme Medical Publishers, 2018), Vol. 44, pp. 20–29.

[9]X. Fu, Z. Su, Y. Wang, A. Sun, L. Wang, X. Deng, Z. Chen, and Y. Fan, "Comparison of hemodynamic features and thrombosis risk of membrane oxygenators with different structures: A numerical study," Comput. Biol. Med. **159**, 106907 (2023).

[10]L. D. Casa, D. H. Deaton, and D. N. Ku, "Role of high shear rate in thrombosis," J. Vasc. Surg. **61**, 1068–1080 (2015).

[11]J. Simons, B. Mees, G. MacLaren, J. F. Fraser, A. M. Zaaqoq, S.-M. Cho, B. M. Patel, D. Brodie, J. Bělohlávek, M. Belliato *et al.*, "Evolution of distal limb perfusion management in adult peripheral venoarterial extracorporeal membrane oxygenation with femoral artery cannulation," Perfusion **39**, 23S–38S (2024).

[12]R. W.-L. Ma, R. L. Huilgol, E. Granger, A. Jackson, S. Saling, A. Dower, and I. Nivison-Smith, "Does a distal perfusion cannula reduce ischaemic complications of extracorporeal membrane oxygenation?," ANZ J. Surg. **86**, 1002–1006 (2016).

[13]Y. Chen, E. Tutungi, J. McMillan, S. M. Tayeh, J. K. Underwood, A. C. Wells, J. A. Smith, and R. A. Moshinsky, "Pressure and flow characteristics of a novel bidirectional cannula for cardiopulmonary bypass," Innovations (Phila) **12**, 430–433 (2017).

[14]T. T. V. Chao and C. H. Lim, "Arterial cannula which allows perfusion along opposing directions within a cannulated vessel," U.S. patent 11,395,869 B2 (26 July 2022); available at https://patents.google.com/patent/US11395869B2/en.

[15]R. Moshinsky, J. McMillan, and E. Tutungi, "Bi-directional perfusion cannula," U.S. patent 8,795,253 B2 (5 August 2014); available at https://patents.google.com/patent/US8795253B2/en.

[16]M. Khamooshi, A. Wickramarachchi, T. Byrne, M. Seman, D. F. Fletcher, A. Burrell, and S. D. Gregory, "Blood flow and emboli transport patterns during venoarterial extracorporeal membrane oxygenation: A computational fluid dynamics study," Comput. Biol. Med. **172**, 108263 (2024).

[17]E. Vignali, E. Gasparotti, D. Haxhiademi, and S. Celi, "Fluid dynamic model for extracorporeal membrane oxygenation support and perfusion in cardiogenic shock," Phys. Fluids **35**, 111909 (2023).

[18]F. Fiusco, F. Rorro, L. M. Broman, and L. Prahl Wittberg, "Numerical and experimental investigation of a lighthouse tip drainage cannula used in extracorporeal membrane oxygenation," Artif. Organs **47**, 330–341 (2023).

[19]Y. Xi, Y. Li, H. Wang, X. Wang, W. Feng, and Z. Chen, "Effect of structural changes in extracorporeal membrane oxygenation return cannulas on hemodynamic performance and blood damage associated with cannulation," Ann. Biomed. Eng. **53**, 1453–1470 (2025).

[20]M. Lui, S. Martino, M. Salerno, and M. Quadrio, "On the turbulence modeling of blood flow in a stenotic vessel," J. Biomech. Eng. **142**, 011009 (2020).

[21]A. R. Pries, D. Neuhaus, and P. Gaehtgens, "Blood viscosity in tube flow: Dependence on diameter and hematocrit," Am. J. Physiol. Heart Circ. Physiol. **263**, H1770–H1778 (1992).

[22]D. M. Eckmann, S. Bowers, M. Stecker, and A. T. Cheung, "Hematocrit, volume expander, temperature, and shear rate effects on blood viscosity," Anesth. Analg. **91**, 539–545 (2000).

[23]K. Patel, D. Palanzo, C. Brehm, J. L. Myers, and A. Ündar, "Hemodynamic evaluation of cannulas for ECMO," in *Cardiopulmonary Bypass* (Elsevier, 2023), pp. 847–865.

[24]Y. Bazilevs, V. M. Calo, J. A. Cottrell, T. J. Hughes, A. Reali, and G. Scovazzi, "Variational multiscale residual-based turbulence modeling for large eddy simulation of incompressible flows," Comput. Methods Appl. Mech. Eng. **197**, 173–201 (2007).

[25]Z. Keshavarz-Motamed, "A diagnostic, monitoring, and predictive tool for patients with complex valvular, vascular and ventricular diseases," Sci. Rep. **10**, 6905 (2020).

[26]K. D. Hodgkiss-Harlow and D. F. Bandyk, "Interpretation of arterial duplex testing of lower-extremity arteries and interventions," Semin. Vasc. Surg. **26**, 95–104 (2013).

[27]W. M. Blackshear, Jr., D. Phillips, and D. Strandness, Jr., "Pulsed Doppler assessment of normal human femoral artery velocity patterns," J. Surg. Res. **27**, 73–83 (1979).
[28]A. M. Malek, S. L. Alper, and S. Izumo, "Hemodynamic shear stress and its role in atherosclerosis," JAMA **282**, 2035–2042 (1999).
[29]K. C. Koskinas, Y. S. Chatzizisis, A. P. Antoniadis, and G. D. Giannoglou, "Role of endothelial shear stress in stent restenosis and thrombosis: Pathophysiologic mechanisms and implications for clinical translation," J. Am. Coll. Cardiol. **59**, 1337–1349 (2012).
[30]Z. M. Ruggeri, "Mechanisms initiating platelet thrombus formation," Thromb. Haemost. **78**, 611–616 (1997).
[31]P. Peruzzo, J. Del Ferraro, and S. Lanzoni, "The importance of hemodynamics in stented vessels: A conceptual model for predicting restenosis using the time-averaged shear stress," Phys. Fluids **36**, 121913 (2024).
[32]G. Marom and D. Bluestein, "Lagrangian methods for blood damage estimation in cardiovascular devices-how numerical implementation affects the results," Expert Rev. Med. Devices **13**, 113–122 (2016).
[33]K. S. Sakariassen, L. Orning, and V. T. Turitto, "The impact of blood shear rate on arterial thrombus formation," Future Sci. OA **1**, FSO30 (2015).
[34]S. Gunaydin, S. Babaroglu, A. B. Budak, B. Sayin, V. Cayhan, and K. Ozisik, "Comparative clinical efficacy of novel bidirectional cannula in cardiac surgery via peripheral cannulation for cardiopulmonary bypass," Perfusion **38**, 44–50 (2023).
[35]M. V. Mascolini, C. G. Fontanella, A. Berardo, and E. L. Carniel, "Influence of trans-urethral catheters on urine pressure-flow relationships in males: A computational fluid-dynamics study," Comput. Methods Programs Biomed. **238**, 107594 (2023).
[36]G. Comunale, L. Di Micco, D. P. Boso, F. M. Susin, and P. Peruzzo, "Numerical models can assist choice of an aortic phantom for in vitro testing," Bioengineering **8**, 101 (2021).
[37]L. Di Micco, G. Comunale, S. Bonvini, P. Peruzzo, and F. M. Susin, "Distensibility of deformable aortic replicas assessed by an integrated in-vitro and in-silico approach," Bioengineering **9**, 94 (2022).
[38]M. Alimohammadi, O. Agu, S. Balabani, and V. Díaz-Zuccarini, "Development of a patient-specific simulation tool to analyse aortic dissections: Assessment of mixed patient-specific flow and pressure boundary conditions," Med. Eng. Phys. **36**, 275–284 (2014).
[39]G. Comunale, P. Peruzzo, B. Castaldi, R. Razzolini, G. Di Salvo, M. A. Padalino, and F. M. Susin, "Understanding and recognition of the right ventricular function and dysfunction via a numerical study," Sci. Rep. **11**, 3709 (2021).
[40]R. Codina, "Stabilization of incompressibility and convection through orthogonal sub-scales in finite element methods," Comput. Methods Appl. Mech. Eng. **190**, 1579–1599 (2000).